Intratumoral *Prevotella copri* Reprograms MARCO$^+$ Tumor-Associated Macrophages by Depleting Glycerophosphocholine to Drive Colorectal Cancer Progression

Qihang Yuan[1,2,3], Yushan Sun[1,2,3], Yue Zhang[1,2,3], Chen Chen[1,2,3], Chenye Bu[1,2,3], Xiaolong Hua[1,2,3], Lejia Sun[1,2,3], Yueming Sun[1,2,3], Zhan Zhang[4], and Yifei Feng[1,2,3]

ABSTRACT

Colorectal cancer is characterized by a complex tumor microenvironment (TME) shaped by intestinal microbiota. In this study, 16S rRNA sequencing of tissues from patients with colorectal cancer identified *Prevotella*, particularly the dominant species *Prevotella copri*, as a key intratumoral bacterium. The parenchymal invasion of *P. copri* was confirmed by FISH, and the abundance of *P. copri* correlated with advanced tumor stages and postoperative serologic markers. Notably, the reduced abundance of *P. copri* in paired normal tissues implied potential bacterial translocation during tumorigenesis. In multiple murine models, *P. copri* not only accelerated tumor growth but also reprogrammed tumor-associated macrophages (TAM) toward a protumoral state. Untargeted metabolomics revealed glycerophosphocholine (GPC) as the only conserved metabolite depleted by *P. copri* across murine models and bacterial cultures, a finding confirmed by spatial metabolomics in clinical specimens. Strikingly, GPC supplementation reprogrammed MARCO$^+$ TAMs toward an antitumoral phenotype, effectively counteracting *P. copri*–mediated tumor progression. Overall, this study uncovers a paradigm in colorectal cancer pathogenesis in which *P. copri* creates an immunosuppressive niche by depleting GPC to manipulate macrophage polarization. These findings position *P. copri* as both a noninvasive diagnostic marker and druggable therapeutic target, with GPC restoration representing a promising immunometabolic intervention strategy.

Significance: Glycerophosphocholine depletion by intratumoral *P. copri* induces immunosuppressive polarization of MARCO$^+$ macrophages in colorectal cancer, revealing a microbial–metabolic–immune axis that remodels the tumor microenvironment and represents a potential immunotherapeutic target.

Introduction

Colorectal cancer ranks among the malignancies with the highest incidence and mortality across the world (1). In recent years, driven by lifestyle changes and an aging population, both the incidence and mortality of colorectal cancer have been steadily increasing globally (2–4). The development of colorectal cancer is influenced by the tumor microenvironment (TME), which is a crucial focus of research (5). The TME is a complex ecosystem comprising various components, including immune cells, stromal cells, extracellular matrix, and microbiota. A deeper understanding of these components and their interactions is essential for developing targeted and personalized therapies for colorectal cancer, thereby improving patient outcomes.

Lately, intratumoral microbiota has emerged as a key component of the TME and has garnered increasing attention (6). For instance, intracellular bacteria in breast cancer tissues have been confirmed to be closely associated with metastasis (7). Although the general gut microbiota operates within the broader intestinal environment, the intratumoral microbiota possesses the potential to engage more directly and deeply in core tumor processes. This unique role of intratumoral microbiota has significant implications for identifying diagnostic biomarkers and potential therapeutic targets. However, the intratumoral microbiota is highly diverse, and its underlying mechanisms are complex, with many aspects still unclear. This complexity presents both opportunities and challenges for advancing our understanding of colorectal cancer progression and developing effective treatments.

In this study, we aimed to investigate the intratumoral microbiota composition across different stages of colorectal cancer using 16S rRNA sequencing. By comparing tumor samples across different stages of colorectal cancer and analyzing adjacent normal tissues, we sought to elucidate the distinct microbial profiles associated with colorectal cancer progression. Our findings revealed that *Prevotella copri* is enriched in colorectal cancer tissues and promotes tumor progression by metabolizing glycerophosphocholine (GPC) to induce M2 macrophage polarization. These results highlight the critical role of intratumoral *P. copri* in colorectal cancer and provide

[1]Department of General Surgery, Colorectal Institute of Nanjing Medical University, The First Affiliated Hospital of Nanjing Medical University, Nanjing, China. [2]Jiangsu Province Engineering Research Center of Colorectal Cancer Precision Medicine and Translational Medicine, Nanjing, China. [3]Collaborative Innovation Center for Cancer Personalized Medicine, Nanjing Medical University, Nanjing, China. [4]Department of Health Inspection and Quarantine, School of Public Health, Key Laboratory of Public Health Safety and Emergency Prevention and Control Technology of Higher Education Institutions in Jiangsu Province, Nanjing Medical University, Nanjing, China.

Q. Yuan, Y. Sun, Y. Zhang, and C. Chen contributed equally to this article.

Corresponding Authors: Yueming Sun, 300 Guangzhou Rd., Gulou, Nanjing 210009, China. E-mail: sunyueming@njmu.edu.cn; Yifei Feng, fengyifei@njmu.edu.cn; and Zhan Zhang, 101 Longmian Ave., Jiangning, Jiangsu 211100, China. E-mail: zhanzhang@njmu.edu.cn

Cancer Res 2026;86:2414–28

doi: 10.1158/0008-5472.CAN-25-3400

new insights into potential therapeutic strategies targeting the tumor microbiome.

Materials and Methods

Human sample collection

A total of 315 frozen colorectal cancer tumor samples (cohort I) were obtained from the tissue bank of Jiangsu Provincial People's Hospital. From this primary cohort, a randomly selected subcohort of 71 tumor samples, for which matched adjacent normal tissue was also available, constituted our paired analysis set. All sample collection was conducted in accordance with the Declaration of Helsinki, with written informed consent obtained from all patients, and was approved by the hospital's ethics committee (2023-SR-212). Tumor samples were collected using sterile surgical blades and disposable sterile forceps immediately after surgical resection of the lesion, whereas paired normal tissues were collected from the area proximal to the lesion in the resected intestinal segment. Additionally, a separate validation set of 10 freshly collected matched tumor–normal pairs (cohort II) was obtained following the same standardized protocols. The characteristics of the patients are detailed in Supplementary Tables S1–S3. Furthermore, one T2N0M0 and one T3N0M0 colorectal cancer specimen were separately obtained for FISH analysis.

16S rRNA sequencing and analysis

Bacterial DNA was extracted from ~100 mg tissue samples, and the 16S rRNA gene V3 to V4 regions were amplified and sequenced on the Illumina MiSeq platform. The raw sequences were processed using the QIIME2 DADA2 pipeline to generate amplicon sequence variants. Downstream analyses, including diversity, taxonomic, and ecological assessments like source tracker (8) and neutral model (9–11), were conducted using R software (version 4.1.3).

P. copri culture

P. copri (strain BNCC337399) was obtained from BeNa Culture Collection (BNCC) and cultured using Columbia blood agar plates and peptone–yeast extract–glucose (PYG) liquid medium composed of 0.5% yeast extract, 0.5% peptone, 0.5% glucose, 0.05% L-cysteine, 0.0005% hemin, and 0.0001% vitamin K1. Both media were prereduced under anaerobic conditions (85% N_2, 10% H_2, and 5% CO_2) for 24 hours. A frozen stock of *P. copri* stored at −80°C was thawed and inoculated onto Columbia blood agar plates, followed by anaerobic incubation at 37°C for 48 hours. Individual colonies were then transferred to PYG liquid medium and cultured anaerobically for additional 48 hours. To expand the culture, the bacterial suspension was subcultured at a 1:10 dilution into fresh PYG medium and incubated until reaching logarithmic phase (OD600 ≈ 0.8). Bacteria were harvested by centrifugation, washed, and resuspended in sterile PBS at a concentration of 5×10^8 colony-forming units (CFU)/mL for subsequent experiments. *P. copri* was grown in PYG medium for 48 hours, and the supernatant was centrifuged at 4,000 rpm for 10 minutes and filtered through a 0.22-μm filter to obtain *P. copri*–conditioned medium (Pc.CM).

Animal experiments

Specific pathogen-free (SPF)–grade male APC$^{min/+}$ mice (5 weeks old) were orally gavaged with *P. copri* (5×10^8 CFU in 0.1 mL sterile saline) three times per week for 12 weeks. GPC was administered in parallel by oral gavage at a dose of 20 μg per mouse, a dosage estimated based on animal model studies, also three times per week in a 0.1 mL saline suspension. Control groups received an equivalent volume of sterile saline (0.1 mL) without *P. copri* or GPC. At the experimental endpoint, mice were euthanized by cervical dislocation under anesthesia.

Two subcutaneous tumor models were established using 6-week-old SPF-grade male C57BL/6J mice. In the first model, mice received oral gavage with *P. copri* (5×10^8 CFU in 0.1 mL sterile saline) for 15 days. On day 15, 1×10^7 MC38 cells suspended in 0.1 mL cold PBS were injected subcutaneously into the right flank of the mice. Oral gavage continued daily until the mice were sacrificed on day 30 (15 days after injection). In the intratumoral bacterial model, MC38 cells were pretreated with *P. copri* at a multiplicity of infection (MOI) of 100 (1×10^9 CFU bacteria per 1×10^7 cells) for 24 hours. On day 15, the pretreated cells were subcutaneously injected into the right flank. Tumor volume was measured daily until sacrifice on day 30 for endpoint analysis.

The macrophage depletion model was established by intraperitoneal injection of clodronate liposomes (refs. 12–15). Six-week-old SPF-grade male APC$^{min/+}$ mice received intraperitoneal injections (200 μL) of clodronate liposomes (5 mg/mL) twice weekly for 8 weeks. Control mice were injected with an equivalent volume of control liposomes. Concurrently, both groups were orally gavaged three times per week with either *P. copri* (5×10^8 CFU in 0.1 mL sterile saline) or GPC (20 μg in 0.1 mL sterile saline). Mice were sacrificed at the end of 8-week treatment period for further analysis.

Detection of *P. copri* using FISH

FISH was performed to confirm *P. copri* colonization in colon or tumor tissues using a DNA FISH Kit (Future Biotech Co., Ltd.; ref. 16), Briefly, paraffin-embedded colon sections (3 μm) were deparaffinized, dehydrated, and denatured, rehydrated through a graded ethanol series, and subjected to denaturation. Hybridization was then carried out using a Cy3-labeled *P. copri*–specific probe (TTTCGCTTGGCCGCTGACCTGTTC) at 37°C for 2 hours in a humidified chamber. After hybridization, slides were washed to remove unbound probe, counterstained with DAPI to visualize nuclei, and mounted. Fluorescent signals were detected and imaged using a confocal laser scanning microscope (Leica).

Histology, IHC, and immunofluorescence

To evaluate the histopathologic changes in APC$^{min/+}$ mice following *P. copri* treatment, formalin-fixed, paraffin-embedded (FFPE) sections of the colon were stained with hematoxylin and eosin (H&E).

Tumor cell proliferation was assessed by IHC staining for Ki67 and proliferating cell nuclear antigen (PCNA). Briefly, 4-μm FFPE tissue sections were deparaffinized, rehydrated, and subjected to antigen retrieval in citrate buffer (pH 6). Endogenous peroxidase activity was quenched with 3% hydrogen peroxide, followed by blocking with 5% normal goat serum. Sections were incubated overnight at 4°C with primary antibodies against Ki67 (Servicebio, AB_3083641) and PCNA (Servicebio, AB_3714654). After washing, sections were incubated with Cy3-conjugated secondary antibodies (Servicebio, AB_2923552) for 1 hour at room temperature. Detection was performed using DAB substrate, and sections were counterstained with hematoxylin.

Tumor sections were immunostained to assess macrophage infiltration and phenotype using antibodies against F4/80 (Servicebio, AB_2938980), CD68 (Servicebio, AB_2924885), CD86 (Servicebio, AB_3661680), CD206 (Servicebio, AB_3665021), and macrophage

receptor with collagenous structure (MARCO; Novus, AB_3585255). Nuclei were visualized with DAPI, and images were captured by confocal microscopy (Leica).

RNA sequencing analysis

Total RNA was extracted from snap-frozen MC38 tumors and sequenced on an Illumina NovaSeq 6000 platform. After quality control (QC) and alignment to the mm10 genome, differential gene expression analysis was performed using DESeq2 ($|\text{fold change}| > 1.2$, $P < 0.05$). Gene set enrichment analysis (GSEA) was subsequently conducted.

Cell culture

Bone marrow–derived macrophages (BMDM) were obtained from tibias and femurs of 6- to 8-week-old C57BL/6 mice. Bone marrow cells were flushed with cold DMEM (Gibco), filtered through a 70-μm strainer, centrifuged at 1,500 rpm for 5 minutes, and resuspended in complete medium consisting of DMEM supplemented with 10% FBS (Gibco) and 1% penicillin/streptomycin (Gibco). Cells were plated and cultured in the presence of 20 ng/mL macrophage colony-stimulating factor (Beyotime, cat. #P6015) for 6 days, with medium refreshed every 2 days. Adherent BMDMs were harvested for subsequent experiments.

The mouse colorectal cancer cell line MC38 and the human colorectal cancer cell line HCT116 were obtained from the Cell Bank of the Chinese Academy of Sciences (CBofCAS; cat. #SCSP-5431 and SCSP-5076, respectively) in March 2023. The human monocytic cell line THP-1 was obtained from the CBofCAS (cat. #SCSP-567) in July 2023. All cell lines were authenticated by short tandem repeat profiling by the bank prior to shipment and were tested negative for *Mycoplasma* contamination using the PCR-based method. The latest in-house *Mycoplasma* test was performed in October 2025, using a Mycoplasma qPCR Detection Kit (Beyotime, cat. #C0303S), and all cell lines were confirmed to be free of contamination.

THP-1 cells were cultured in RPMI-1640 medium (Gibco) supplemented with 10% FBS and 1% penicillin/streptomycin. Differentiation into macrophage-like cells was induced with 100 ng/mL phorbol 12-myristate 13-acetate (PMA; Beyotime, cat. #S1819) for 48 hours, followed by a 24-hour stabilization period in fresh medium prior to use. MC38 and HCT116 cells were maintained in DMEM supplemented with 10% FBS and 1% penicillin/streptomycin. All cells were cultured at 37°C in a humidified incubator with 5% CO_2. For all experiments, cells were used within a cumulative period of 6 weeks after thawing, which corresponded to a total of approximately 10 passages.

Cell Counting Kit-8 assay

MC38 cells or HCT116 cells were seeded into a 96-well plate at a density of 5,000 cells per well in 100 μL of complete DMEM and incubated overnight in an incubator at 37°C with 5% CO_2. Cells were subsequently treated with one of the following: Pc.CM (8 μL per well), heat-killed *P. copri* (5×10^5 CFU per well), or GPC (100 μg per well) for 5 days. Treatments were maintained for 5 days. BMDMs or PMA-differentiated THP-1 cells were seeded into a six-well plate at a density of 100,000 cells per well. Cells were stimulated with Pc.CM (8 μL per well), heat-killed *P. copri* (5×10^5 CFU per well), or GPC (100 μg per well) for 48 hours. After stimulation, culture supernatants (10 μL per well) were collected to treat seeded MC38 or HCT116 cells (5,000 cells/well) for another 24 hours. Cell viability was assessed daily using the Cell Counting Kit-8 (Beyotime, cat. #C0037) following the manufacturer's instructions. Absorbance was measured at 450 nm using a microplate reader.

Cell cycle analysis

To assess the impact of macrophage-derived factors on tumor cell proliferation, cell cycle analysis was performed using flow cytometry (FCM). For the cell cycle, HCT116 cells were seeded at 2×10^5 cells per well in the lower chamber of six-well Transwell plates and synchronized by serum deprivation for 24 hours. In the upper chamber, PMA-differentiated THP-1 cells (1×10^5 cells per well) were treated with PBS (control), Pc.CM, GPC (100 μg per well), or GPC-supplemented Pc.CM for 24 hours. After treatment, coculture was established by placing the upper chamber with THP-1 cells above the synchronized HCT116 cells for an additional 48 hours.

HCT116 cells were then harvested and fixed with 70% ethanol at 4°C overnight. Following fixation, cells were washed with PBS, treated with RNase A (50 μg/mL) at room temperature for 15 minutes, and stained with propidium iodide (50 μg/mL) for 30 minutes in the dark. DNA content was analyzed using a FACSCalibur flow cytometer (BD Biosciences) equipped with a 488-nm laser and a 585-/540-nm bandpass filter. Cell cycle distribution (G_0–G_1, S, and G_2–M phases) was determined using ModFit LT software (Verity Software House).

Isolation of immune cells

Tumor tissues were enzymatically dissociated into single-cell suspensions using the Tumor Dissociation Reagent Kit (Miltenyi Biotec), following the manufacturer's instructions. Briefly, tumors were minced into small fragments and then incubated with the enzyme cocktails at 37°C. The resulting suspensions were filtrated through a 100-μm cell strainer to remove debris and undigested material. Cells were centrifuged at 300 *g* for 5 minutes at 4°C, and the pellet was resuspended in PBS containing 1% BSA.

qPCR

Total RNA was extracted from cells or tissues using standard protocols. RNA was reverse transcribed into cDNA using a reverse transcriptase enzyme. qPCR was performed using specific primers for the target genes (Supplementary Table S4). The expression levels of target genes were normalized to an internal reference gene and analyzed using the $2^{-\Delta\Delta Ct}$ method.

Untargeted metabolomics profiling

Serum samples from $APC^{min/+}$ mice, subcutaneous tumor models, and Pc.CM were analyzed by untargeted metabolomics using LC/MS-MS (Waters). Metabolites were extracted with ice-cold methanol, and QC samples were integrated throughout the randomized sequence. Data were acquired in both ESI-positive and -negative modes. Raw data processing, metabolite identification, and annotation were performed using XCMS and metaX. Differential metabolites were identified and subjected to Kyoto Encyclopedia of Genes and Genomes (KEGG) pathway analysis.

Quantification of GPC

Fecal samples from $APC^{min/+}$ mice were weighed, homogenized by ultrasonication, and stabilized through freezing. GPC levels were then quantified using an high-performance liquid chromatography coupled with evaporative light scattering detection (HPLC-ELSD) system (Shimadzu, LC-20A), with a commercial standard (TRC, #G598700) for calibration.

Spatial metabolomics sample processing and analysis

Tumor and adjacent normal tissues (not separated) were collected without formalin fixation, with each sample measuring approximately 0.8 to 1 cm in diameter. The samples were stored in an ultralow temperature freezer at −80°C. Before sectioning, the tissues were embedded in Cryo-Gel and sectioned into 8- to 10-μm-thick cryosections using a precooled cryostat (Leica, CM1860), which were then adhered to positively charged slides (Fisher Superfrost Plus). Routine pathologic sections were also prepared for H&E staining. Subsequently, spatial metabolomics analysis was performed using atmospheric pressure matrix-assisted laser desorption ionization coupled with a mass spectrometer (Thermo Fisher Scientific, QE PLUS). Intelligent region selection and functional analysis were conducted using proprietary algorithms, and ion spatial imaging maps were generated using Mzkit software. Metabolite identification was performed by matching against databases such as KEGG, Human Metabolome Database, LipidMaps, and MoNA. Regional conservation typing was based on the motif sequence search principle using the Gibbs sampling algorithm.

FCM

A single-cell suspension from dissociated tumor tissue or isolated BMDMs was first stained with Fixable Viability Stain 780 (APC-cy7, BD Biosciences, AB_2869673) to distinguish live and dead cells. Cells were incubated with the viability stain at 37°C in the dark for 8 minutes, followed by washing with PBS. Subsequently, cells were stained with fluorochrome-conjugated antibodies against CD45 (BV510, BD Biosciences, AB_2739896), CD11b (PE, BD Biosciences, AB_396680), F4/80 (BV421, BD Biosciences, AB_2734779), and CD86 (BV650, BD Biosciences, AB_2738665), as well as MARCO (FITC, Novus, AB_3123344). This staining was performed on ice in the dark for 30 minutes. After washing with PBS, cells were fixed and permeabilized using the BD Fixation/Permeabilization Kit (AB_2869008) according to the manufacturer's instructions. Cells were then stained with anti-CD206 (AF647, BD Biosciences, AB_2739133) on ice in the dark for an additional 30 minutes. Finally, cells were washed and resuspended in PBS containing 1% FBS for analysis. FCM analysis was performed using a FACSymphony A5 flow cytometer (BD Biosciences), equipped with five lasers and 23 detectors, allowing for high-dimensional resolution of immune cell subsets. Tumor-associated macrophages (TAM) were classified as M1-like (CD11b$^+$F4/80$^+$CD86$^+$) or M2-like (CD11b$^+$F4/80$^+$CD206$^+$) populations. Gates and quadrants were based on fluorescence minus one control (Supplementary Fig. S1).

Molecular docking

Molecular docking was performed using AutoDock Vina with the prepared 2OY3 protein structure (extracted from PDB complex using PyMOL). The ligand compound was docked into the binding site, with the best pose (docking score: −5.944 kcal/mol) showing compound (cyan sticks) forming hydrogen bonds (yellow dashes) with key residues (brick red sticks).

MARCO knockdown and Western blotting

The MARCO-targeting short hairpin RNA sequence (5′-GATGATGATTGGGATAATAAT-3′) was cloned into the lentiviral vector LV1. BMDMs were seeded at a density of 1×10^5 cells per well in a six-well plate. The lentivirus was then used to transduce BMDMs at an MOI of 10 in the presence of 5 μg/mL polybrene to enhance transduction efficiency. Knockdown efficiency was confirmed by Western blotting. Briefly, total protein was extracted from cells, quantified, separated by SDS-PAGE, and transferred to a polyvinylidene difluoride or nitrocellulose membrane. The membrane was blocked with 5% nonfat milk in TBST for 1 hour at room temperature. Then, it was incubated with MARCO antibody (Novus, AB_2140593) at a dilution of 0.25 μg/mL overnight at 4°C. After washing, the samples were incubated with the secondary antibody (GB122199, Servicebio, Goat Anti-Rabbit IgG HRP, dilution 1:500) for 1 hour at room temperature. Protein bands were visualized using chemiluminescence with an enhanced chemiluminescence substrate kit (Thermo Fisher Scientific, cat. #32106).

Statistical analysis

Data were expressed as mean ± SD. Statistical analyses were conducted with R software (version 4.1.3). Normality test was conducted prior to the following analysis. For data that followed a normal distribution, they were analyzed by one-way ANOVA or Student *t* test; for those that did not follow a normal distribution, they were compared by a Mann–Whitney *U* test or Kruskal–Wallis test. Tumor volume, weight, and other measurement data were analyzed using repeated-measures ANOVA.

Ethics approval

Human studies were approved by the Ethics Committee of Jiangsu Provincial People's Hospital (2023-SR-212) with written informed consent from all participants. Animal experiments complied with NIH guidelines and were approved by the Laboratory Animal Welfare and Ethics Committee of Nanjing Medical University (IAUC-2403024).

Results

Prevotella in TME is significantly associated with T-stage in colorectal cancer

To explore the intratumoral microbiota composition in different stages of colorectal cancer and identify bacterial components associated with tumor progression, we conducted 16S rRNA gene sequencing on tumor samples from 315 treatment-naïve patients with colorectal cancer (Supplementary Table S1) stratified by T-stage. Species accumulation curves confirmed adequate sequencing depth (Supplementary Fig. S2A). Significant differences in microbial composition were observed between T0 to T2 (early stage) and T3 to T4 (advanced stage) groups in terms of α and β diversity (**Fig. 1A**; Supplementary Fig. S2B). Strikingly, with potential contamination ruled out, microbiota profiling revealed that *Prevotella*, a conditionally pathogenic bacterium, is a significant component of the TME (**Fig. 1B**; Supplementary Fig. S2C), and the *Prevotella*-dominant enterotype was overrepresented in T3 to T4 cases (**Fig. 1C**). Taxonomic analysis further identified *Prevotella* as the most differentially abundant genus (**Fig. 1D**; Supplementary Fig. S2D), with its relative abundance escalating proportionally to T-stage (**Fig. 1E**). Together, these data establish *Prevotella* as a tumor stage–associated genus within the colorectal cancer microbiota. Additionally, IHC staining revealed significantly higher Ki67$^+$ proliferative indices in tumors harboring elevated *Prevotella* levels (**Fig. 1F**). Further analysis of paired pre-/postoperative serum markers showed that T3 to T4 patients in the *Prevotella*-high group exhibited a smaller relative decrease in carcinoembryonic antigen and CA19-9, but not α-fetoprotein levels, compared with *Prevotella*-low cases (**Fig. 1G** and **H**; Supplementary Fig. S2E). These findings suggest an association between *Prevotella*, as a prevalent TME constituent, and colorectal cancer progression.

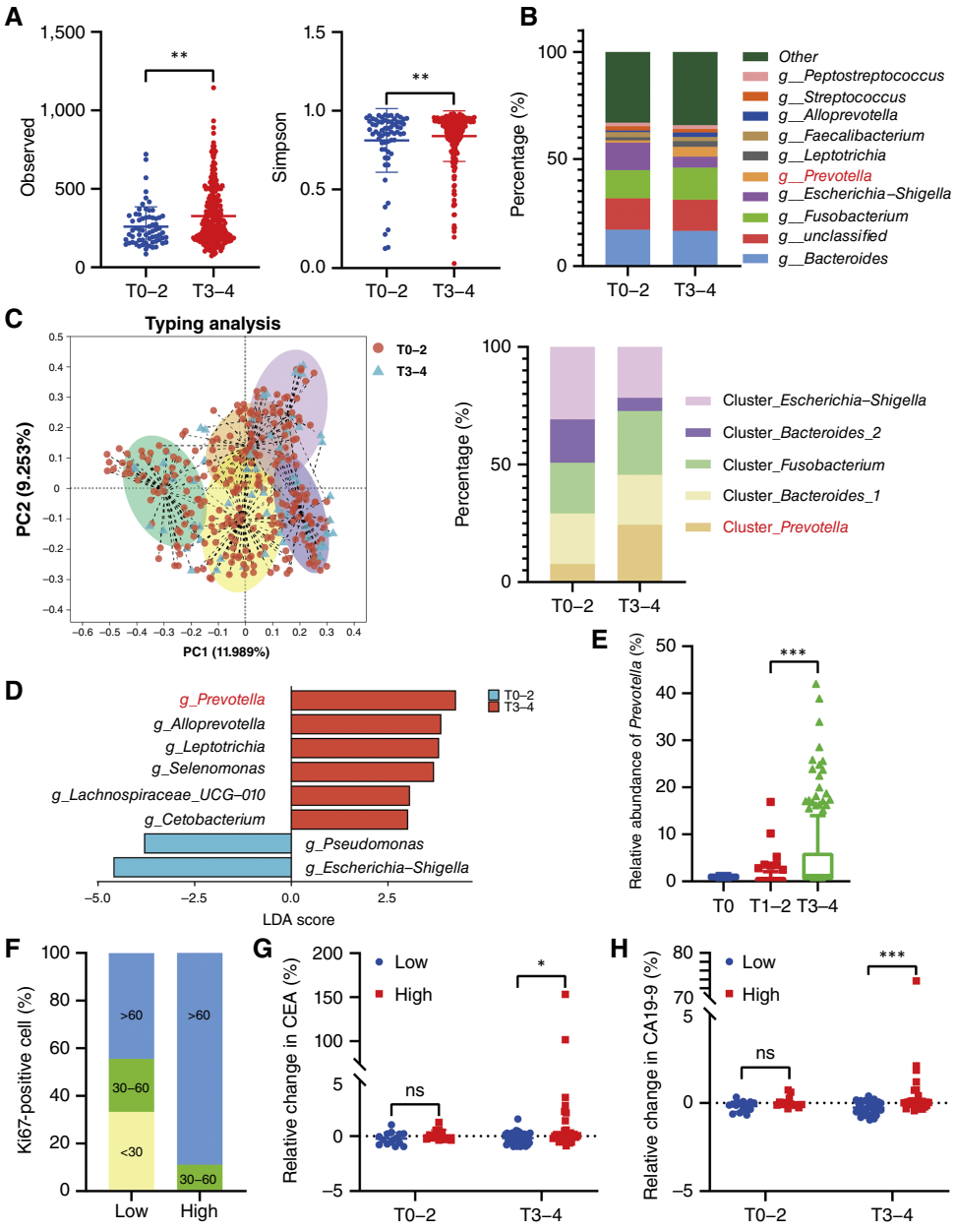

Figure 1.

The intratumoral abundance of *P. copri* in association with colorectal cancer progression. **A,** α diversity metrics of in-house 16S rRNA sequencing data of colorectal cancer tumor tissues. **B,** Stacked bar chart showing the mean relative abundance of the top 10 genera (selected by median abundance across all samples) within each group (T0–2, $n = 65$; T3–4, $n = 250$). **C,** Typing analysis is shown by principal component (PC) analysis, and the percentage of enterotypes was statistically analyzed using a stacked bar chart. **D,** Enriched genera analysis by LEfSe [linear discriminant analysis (LDA) score >2.5]. **E,** The relative abundance of *Prevotella* increases with higher T stages (Kruskal–Wallis test). **F,** The proportion of different percentages of Ki67$^+$ cells in patients with colorectal cancer with high and low abundance of *P. copri*. **G,** T3 to T4 patients ($n = 65$) with high *P. copri* abundance (Pc high) showed a smaller relative reduction [(postoperative value − preoperative value)/preoperative value] in postoperative carcinoembryonic antigen levels compared with the Pc-low group, whereas no such difference was observed in T0 to T2 patients ($n = 27$). CEA, carcinoembryonic antigen. **H,** Similar trends were observed for CA19-9. Low, *Prevotella* low (<median); high, *Prevotella* high (≥median). Data are expressed as mean ± SD. ns, nonsignificant; *, $P < 0.05$; **, $P < 0.01$; ***, $P < 0.001$. .

Distribution of *Prevotella* in tumor and normal microenvironments

Building on our identification of *Prevotella* as a colorectal cancer–associated bacterium, the spatial organization of intratumoral microbiota and their ecological relationships with adjacent normal tissues require further elucidation. To address this, we performed 16S rRNA sequencing on 71 randomly selected paired adjacent normal tissues (Supplementary Table S2) from cohort I. β diversity analysis revealed significant compositional differences between T and N tissues (**Fig. 2A**), promoting systematic investigation into microbial translocation dynamics.

The public metagenomic datasets (PRJDB4176 and PRJEB7774) revealed that *P. copri* is the dominant species within this genus in the human gut and is consistently associated with advanced colorectal cancer (Supplementary Fig. S2F and S2G). To delineate the spatial distribution of *P. copri* in colorectal cancer microenvironments, we performed FISH with *P. copri*–specific probes on paired tumor/normal tissues from cohort II (Supplementary Table S3). Strikingly, *P. copri* exhibited restricted distribution in normal tissues but demonstrated deep parenchymal infiltration in tumors and showed positive association with T-stage (**Fig. 2B** and **C**; Supplementary Fig. S2H). Given these findings, we next analyzed the relationship between tumor microbiota and adjacent normal tissues. SourceTracker analysis demonstrated that 96.3% of intratumoral bacteria originated from adjacent N tissues, with this proportion increasing to 96.8% in T3 to T4 patients (**Fig. 2D**).

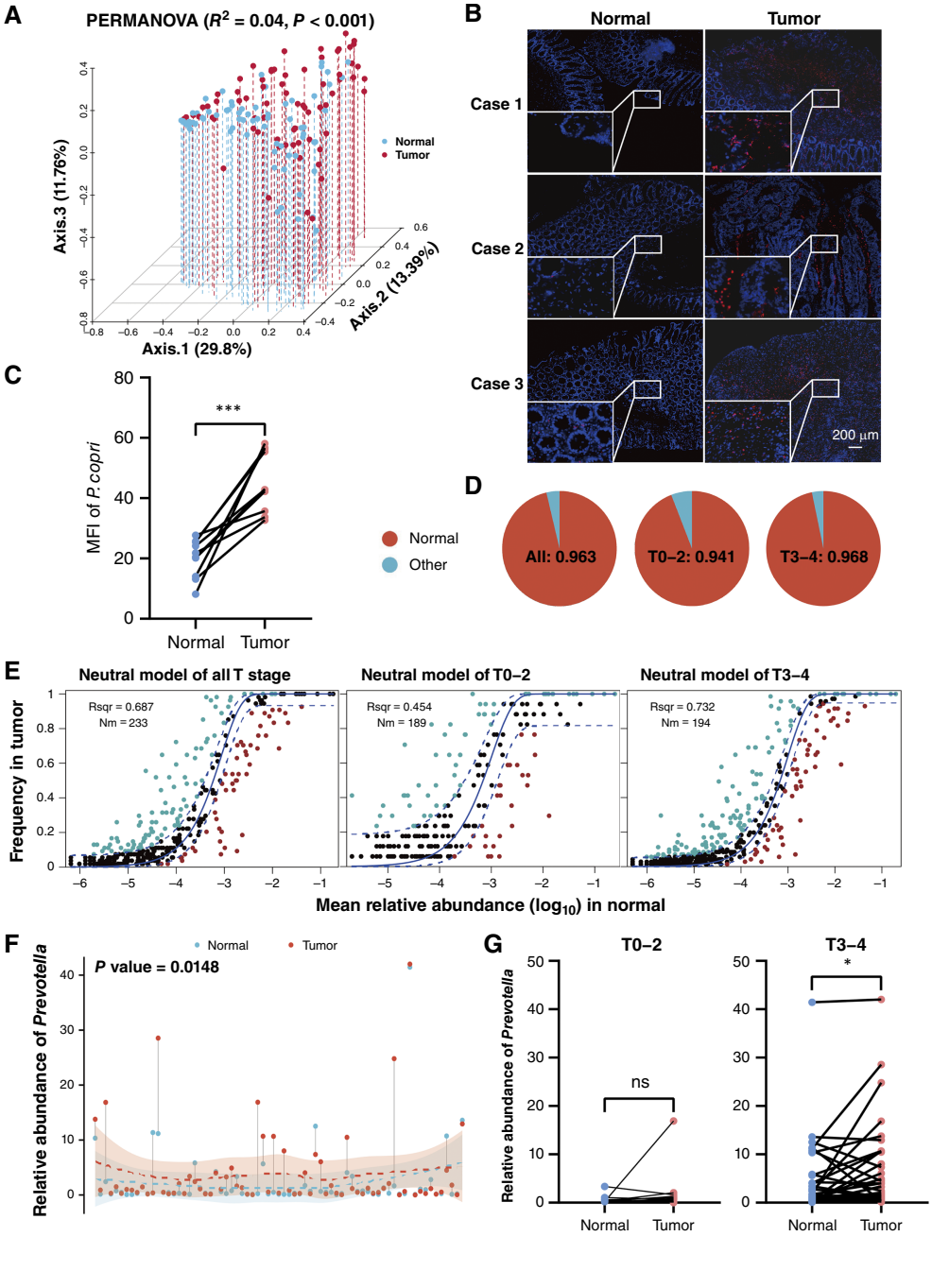

Figure 2.

Enrichment and source analysis of *P. copri* in tumor tissues. **A,** β diversity is shown by principal coordinate analysis, and the statistical difference was analyzed by PERMANOVA (R^2 = 0.04, F = 5.783, P < 0.001). **B,** Representative FISH images of *P. copri* in paired primary tumor and adjacent normal tissues from patients with colorectal cancer; insets show higher-magnification views of the corresponding boxed regions. **C,** FISH signal intensity of *P. copri* in paired primary tumor and adjacent normal tissues (n = 10). MFI, mean fluorescence intensity. **D,** The SourceTracker results are displayed using a pie chart, in which the red portion represents the proportion of intratumoral bacteria originating from normal colonic microbiota. **E,** Neutral model fitting results using normal colonic microbiota as the source. The solid blue line represents the fitted curve, and the dashed blue lines indicate the 95% confidence interval. The coefficient of determination (R^2) measures the goodness of fit for the neutral model, ranging from ≤0 (no fit) to 1 (perfect fit). **F,** Dumbbell plot comparing the abundance of *Prevotella* between tumor sites and normal colonic sites in paired patient samples. **G,** *Prevotella* abundance in tumor and normal tissues from patients with colorectal cancer with T0 to T2 and T3 to T4 stage. Data are expressed as mean ± SD. Compared with normal tissue, *, P < 0.05; ***, P < 0.001; ns, nonsignificant.

The Tumor–Normal Neutral model (Supplementary Fig. S2I) further corroborated this migration trend, demonstrating a stronger fit in T3 to T4 compared with T0 to T1 groups (**Fig. 2E**). Collectively, these findings paint a coherent picture in which tumor-associated microbiota arise through dynamic migration from adjacent tissues, with *P. copri*'s spatial redistribution exemplifying how T-stage progression reshapes microbial ecology. Notably, paired analysis identified significant enrichment of *Prevotella* in T compared with N tissues (**Fig. 2F**), with the disparity being markedly greater in T3 to T4 patients (**Fig. 2G**). This observation was consistent with the broader pattern of T-stage–dependent microbial migration, indicating that *Prevotella* may contribute to the evolving ecological dynamics of the TME during colorectal cancer progression.

P. copri promoted colorectal cancer progression in mouse models

Given the association of *Prevotella* with advanced colorectal cancer, we focused on its dominant species (17), *P. copri*, to investigate its functional role in tumor progression. To address this, APC$^{min/+}$ mice and subcutaneous tumor-bearing mouse models were treated with *P. copri*. After 12 weeks of treatment, *P. copri*–colonized APC$^{min/+}$ mice exhibited significantly higher tumor burden and

splenomegaly compared with both untreated and *E. coli*–treated groups (**Fig. 3A–D**). 16S rRNA sequencing of mouse feces confirmed the successful and specific colonization of *P. copri* (**Fig. 3E**). No notable alterations in other pathogenic or probiotic bacteria were observed (Supplementary Fig. S3A and S3B). Furthermore, FISH analysis validated these findings, revealing a higher bacterial load of *P. copri* in the treated group. Moreover, we observed a specific enrichment of *P. copri* within the tumor areas (**Fig. 3F**), a finding that mirrors the enrichment pattern we identified in human colorectal cancer samples. To ensure reproducibility, subcutaneous tumor models were established in C57BL/6 mice, *P. copri* was introduced by either oral gavage or an intratumoral bacterial model, and successful bacterial survival within tumor cells was confirmed prior to these experiments (Supplementary Fig. S3C). Both routes of administration significantly accelerated tumor growth and induced splenomegaly (**Fig. 3G–J** for the oral gavage model and **K–N** for the intratumoral bacterial model). Given that splenomegaly often indicates immune disruption, this finding suggests a potential role of *P. copri* in modulating the host immune microenvironment.

Independent replicate experiments validated the key phenotypic findings of *P. copri*–driven tumor progression in both the $APC^{min/+}$ model (Supplementary Fig. S4A–S4F) and in subcutaneous models employing either oral gavage (Supplementary Fig. S4G–S4K) or the intratumoral bacterial model (Supplementary Fig. S4L–S4P). Together, these results provide strong evidence that *P. copri* promotes colorectal tumor development *in vivo*.

P. copri drives colorectal cancer progression by modulating macrophage polarization

Our findings above demonstrated the tumor-promoting effects of *P. copri in vivo*; however, no direct effect on cancer cells was observed *in vitro* (Supplementary Fig. S5A), suggesting an indirect mechanism, such as tumor immunity or tumor metabolism.

To elucidate the underlying mechanism, we performed transcriptome sequencing on subcutaneous tumors from the intratumoral bacterial model and PBS-treated control mice. GSEA revealed a striking downregulation of multiple immune-related pathways, including TNFα–NFκB, IL6–JAK–STAT3, inflammatory response, and IFNγ response signaling pathways, upon *P. copri* treatment (**Fig. 4A**). Differential analysis also revealed significant expression changes in numerous tumor immunity–related genes. Notably, we observed alterations in genes related to macrophage polarization, including the downregulation of *CD86* and *Nos2*, as well as the upregulation of *Mrc1* and *Cd209a*, among others, in the intratumoral bacterial model group (**Fig. 4B**).

Indeed, emerging reports have highlighted the critical role of TAMs in bridging the relationship between microbiota and tumor progression (18). Furthermore, immunofluorescence analysis showed a significant increase in $F4/80^+$ cells in both subcutaneous tumor models (**Fig. 4C** and **D**). FCM of tumor tissues from *P. copri*–gavaged $APC^{min/+}$ mice revealed a shift of macrophages from an M1 ($CD86^+$) to an M2 ($CD206^+$) phenotype (**Fig. 4E** and **F**). The functional importance of macrophages was confirmed by depletion experiments using clodronate liposomes, which substantially abrogated the tumor-promoting effect of *P. copri* (**Fig. 4G–J**), establishing macrophages as a critical mediator. Multicolor immunofluorescence analysis of human colorectal cancer tissues further validated these findings, showing that high *P. copri* signal intensity correlated with an increased M2/M1 macrophage ratio (**Fig. 4K**). We next dissected this macrophage-mediated mechanism *in vitro*. The supernatant from cultured macrophages pretreated with live *P. copri* significantly enhanced colorectal cancer cell proliferation (Supplementary Fig. S5B). Similarly, although Pc.CM alone exerted no direct effect on colorectal cancer cells (Supplementary Fig. S5C and S5D), supernatants from Pc.CM-pretreated macrophages significantly promoted tumor cell growth (Supplementary Fig. S5E). This confirms the essential role of macrophages as other immune cell populations remained unaffected *in vivo* (Supplementary Fig. S5F and S4G). Furthermore, Pc.CM also promoted cell-cycle progression (Supplementary Fig. S5H). FCM of BMDMs confirmed that Pc.CM alone was sufficient to recapitulate the M2-polarizing shift observed *in vivo* (Supplementary Fig. S5I and S5J). Collectively, our results indicate that Pc.CM may contain key components that drive macrophage polarization.

P. copri–derived intratumoral GPC depletion promotes colorectal cancer by driving M2 macrophage polarization

In light of above findings that the effects observed could be attributed to *P. copri*'s active products in Pc.CM, untargeted metabolomics profiling was employed to screen potential components both *in vitro* and *in vivo*. Distinct metabolic signatures were observed in serum from *P. copri*–gavaged $APC^{min/+}$ mice, serum from the intratumoral bacterial model, and Pc.CM samples (**Fig. 5A–C**). Notably, GPC, a water-soluble acetylcholine precursor, was the only metabolite consistently depleted across all three models, without significant disruption in the GPC metabolism gene of host (**Fig. 5D** and **E**, related metabolites in **Fig. 5F**; Supplementary Fig. S6A–S6E). Subsequent quantification by HPLC-ELSD further confirmed decreased fecal GPC in *P. copri*–gavaged $APC^{min/+}$ mice (**Fig. 5G**). This fecal decrease mirrors the GPC reduction observed with serum *in vivo* and Pc.CM *in vitro*, suggesting that *P. copri* can directly lower GPC levels. Moreover, we collected a colorectal cancer specimen with adjacent nontumor tissue from a patient with stage III for spatial metabolomics analysis. After H&E staining and tumor region demarcation (**Fig. 5H**), we observed a significant depletion of GPC within the tumor area compared with the adjacent nontumor area within the same specimen (**Fig. 5I** and **J**), further highlighting the potential role of GPC in tumor progression. Additionally, we also performed KEGG pathway analysis, which highlighted enrichment in glycerophospholipid metabolism pathways (**Fig. 5K** and **L**; Supplementary Fig. S6F). These metabolomics results indicate that depletion of GPC may be a potential mechanism through which *P. copri* fuels colorectal cancer progression.

Given that GPC is a key component decreased in Pc.CM, its multifaceted roles were investigated. GPC effectively reversed the promotion of tumor cell proliferation and cell-cycle progression induced by macrophages pretreated with Pc.CM (Supplementary Fig. S7A–S7C). Additionally, GPC upregulated M1-like macrophage-related genes, such as *Tnfα*, *IL1β*, and *IL6*, while downregulating M2-like markers, including *Cd206*, *Arg1*, and *Mgl1* (**Fig. 6A**). These findings were consistent with the FCM results of macrophage polarization following *in vitro* stimulation (**Fig. 6B** and **C**). Furthermore, GPC significantly inhibited colorectal cancer progression in $APC^{min/+}$ mice and alleviated splenomegaly, thereby counteracting the tumor-promoting effects of *P. copri* (**Fig. 6D–G**). FCM analysis of tumor tissues revealed a shift in macrophage polarization toward an M1-like phenotype (**Fig. 6H** and **I**), mirroring the observations *in vitro*.

To determine whether macrophages serve as a critical node through which GPC modulates the TME, we established a macrophage-depleted $APC^{min/+}$ mouse model via intraperitoneal injection of clodronate liposomes (**Fig. 6J**). As expected, macrophage

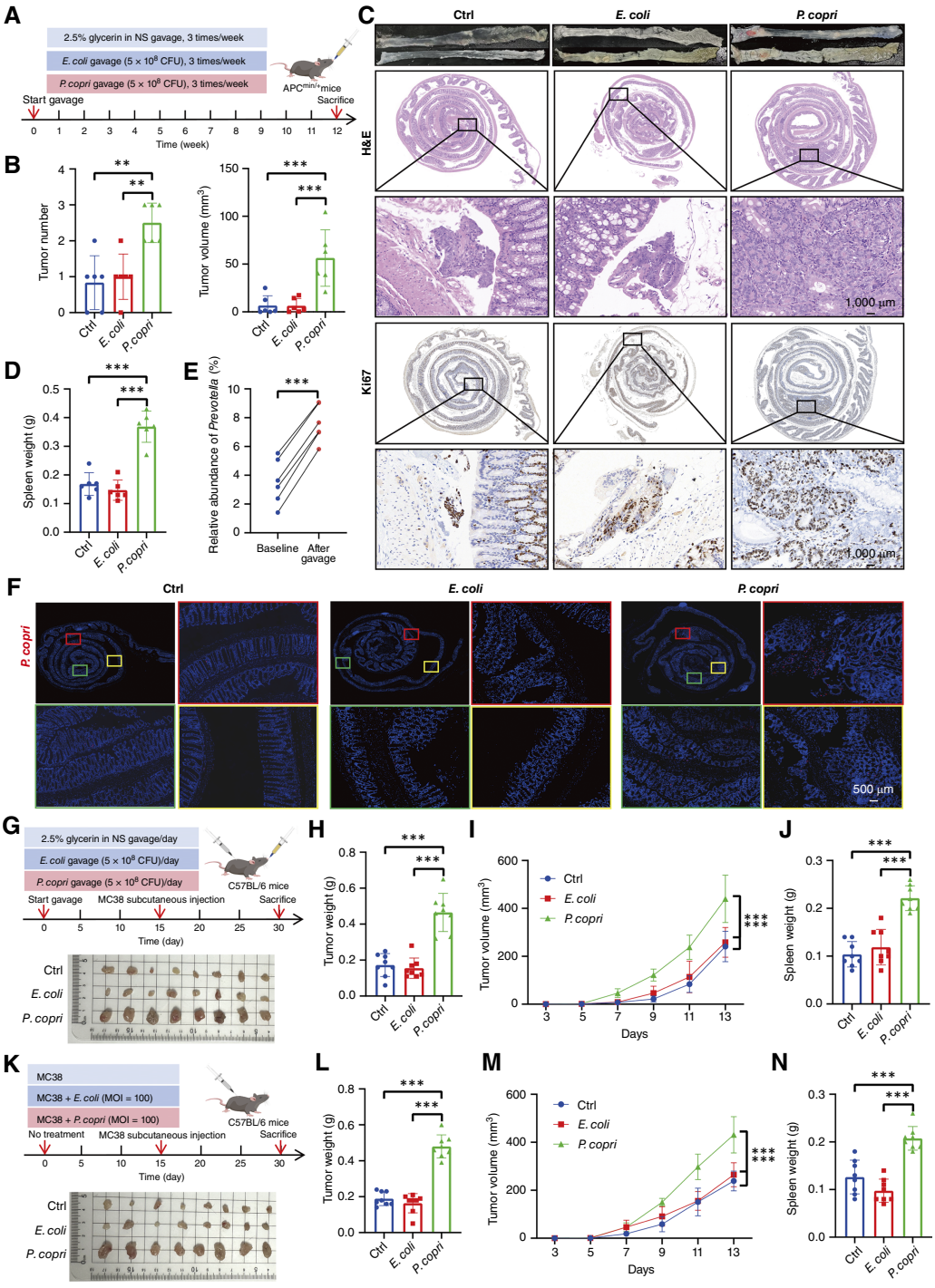

Figure 3.

P. copri promotes colorectal cancer progression *in vivo*. **A,** APC$^{min/+}$ mice received oral gavage of *P. copri* starting at 5 weeks of age, whereas the control group received saline or *E. coli* for 12 weeks ($n = 6$ per group; another independent replicate experiment is shown in Supplementary Fig. S4A). **B,** Number and volume of colorectal tumor. **C,** Colon images of APC$^{min/+}$ mice, with representative histologic sections showing H&E staining and Ki67 IHC of colon tissues. **D,** The relative abundance of *P. copri* in the 16S sequencing of mouse feces before and after *P. copri* gavage. **E,** Spleen weight of APC$^{min/+}$ mice. **F,** Representative images of *P. copri* colonization in colon by FISH. **G,** In the subcutaneous tumor model, C57BL/6 mice were pretreated with *P. copri* via gavage before MC38 cell injection ($n = 8$ per group; another independent replicate experiment is shown in Supplementary Fig. S4G). **H** and **I,** Weight and volume of tumor of C57BL/6 mice. **J,** Spleen weight of subcutaneous tumor-bearing mice following *P. copri* gavage. **K,** Subcutaneous tumors were established in C57BL/6 mice by inoculation of MC38 cells that had been pretreated with *P. copri* (MOI = 100 and 24-hours coculture; $n = 8$ per group; another independent replicate experiment is shown in Supplementary Fig. S4L). **L** and **M,** Weight and volume of tumor of C57BL/6 mice. **N,** Spleen weight of subcutaneous tumor-bearing mice with intratumoral *P. copri*. Data are expressed as mean ± SD. Compared with the control group, **, $P < 0.01$; ***, $P < 0.001$.

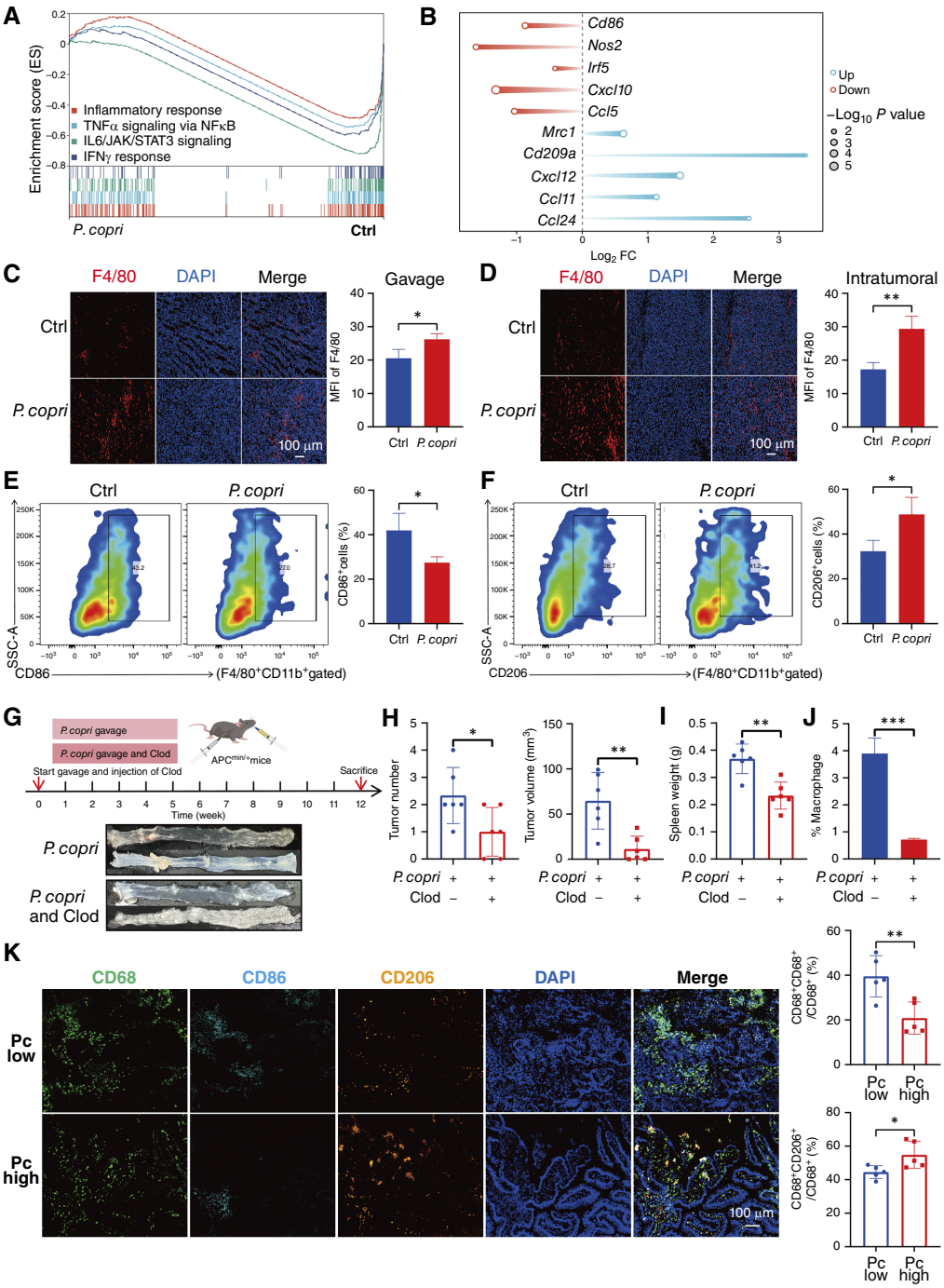

Figure 4.

P. copri promotes colorectal cancer progression by regulating macrophage polarization. **A,** GSEA enrichment analysis of RNA sequencing data reveals changes in tumor immunity–related pathways in subcutaneous tumor with intratumoral *P. copri*. **B,** Differential expression of macrophage polarization–related genes [$P < 0.05$ and fold change (FC) >1.2]. **C** and **D,** Immunofluorescence staining of F4/80 in tumor tissues from oral gavage (**C**) and the intratumoral bacterial (**D**) models. MFI, mean fluorescence intensity. **E** and **F,** FCM analysis of $CD86^+$ macrophage (**E**) and $CD206^+$ macrophage (**F**) in *P. copri*–treated $APC^{min/+}$ mice. **G,** $APC^{min/+}$ mice received *P. copri* ± weekly clodronate liposome injections for macrophage depletion ($n = 6$ per group). **H,** Number and volume of colorectal tumor. **I** and **J,** Spleen weight (**I**) and percentage of macrophages (**J**) in $APC^{min/+}$ mice. **K,** Immunofluorescence of TAMs in human colorectal cancer tissues (Supplementary Table S3) with high vs. low *P. copri* signal intensity (Pc high vs. Pc low). Data are expressed as mean ± SD. Compared with the control group, *, $P < 0.05$; **, $P < 0.01$; ***, $P < 0.001$. Clod, clodronate liposomes.

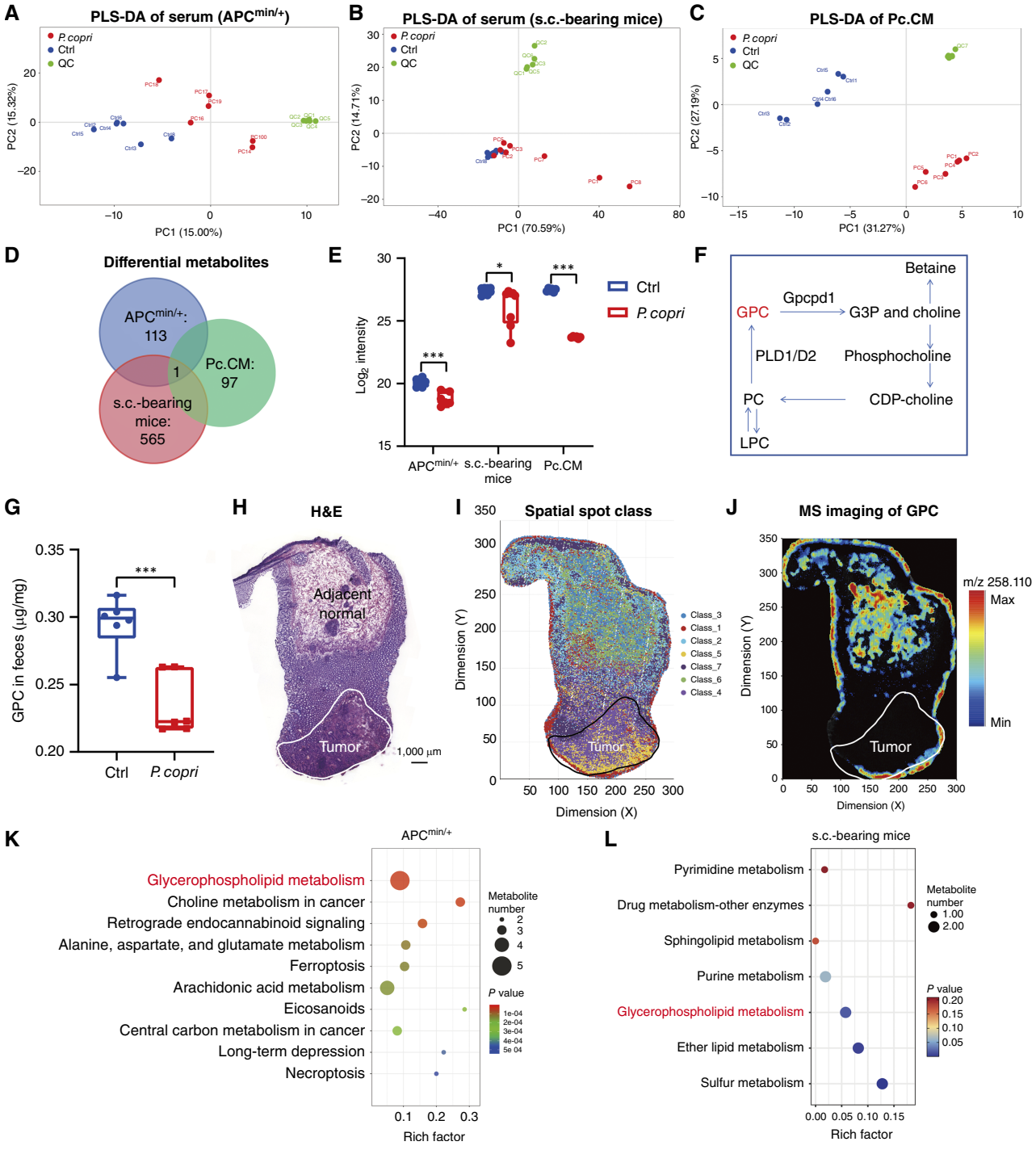

Figure 5.

Discovery of GPC as a key metabolite mediating the effects of *P. copri* on macrophages. **A** and **B,** PLS-DA plots of serum metabolic profiles from *P. copri*–gavaged APC$^{min/+}$ mice (**A**) and subcutaneous tumor-bearing mice (**B**) with intratumoral *P. copri*. PC, principal component. **C,** PLS-DA plots of metabolic profiles of Pc.CM. **D,** Venn diagram of differential metabolites among APC$^{min/+}$ mice serum, C57BL/6 mice serum, and Pc.CM. **E,** Relative abundance of GPC (log_2 -transformed intensity) in serum from *P. copri*–gavaged APC$^{min/+}$ mice, serum from C57BL/6 mice in the intratumoral bacterial models, and Pc-CM. **F,** GPC metabolic pathway. **G,** Quantitative analysis of fecal contents of GPC in *P. copri*–gavaged APC$^{min/+}$ mice. **H–J,** The H&E staining image of the spatial metabolomics sample (**H**), the regional conservation typing map based on the Gibbs sampling algorithm (**I**), and the single-molecule spatial imaging map of GPC (**J**). **K** and **L,** KEGG pathway enrichment analysis of differential serum metabolites in *P. copri*–treated APC$^{min/+}$ mice (**K**) and subcutaneous tumor-bearing mice (**L**). Compared with the control group, *, $P < 0.05$; ***, $P < 0.001$.

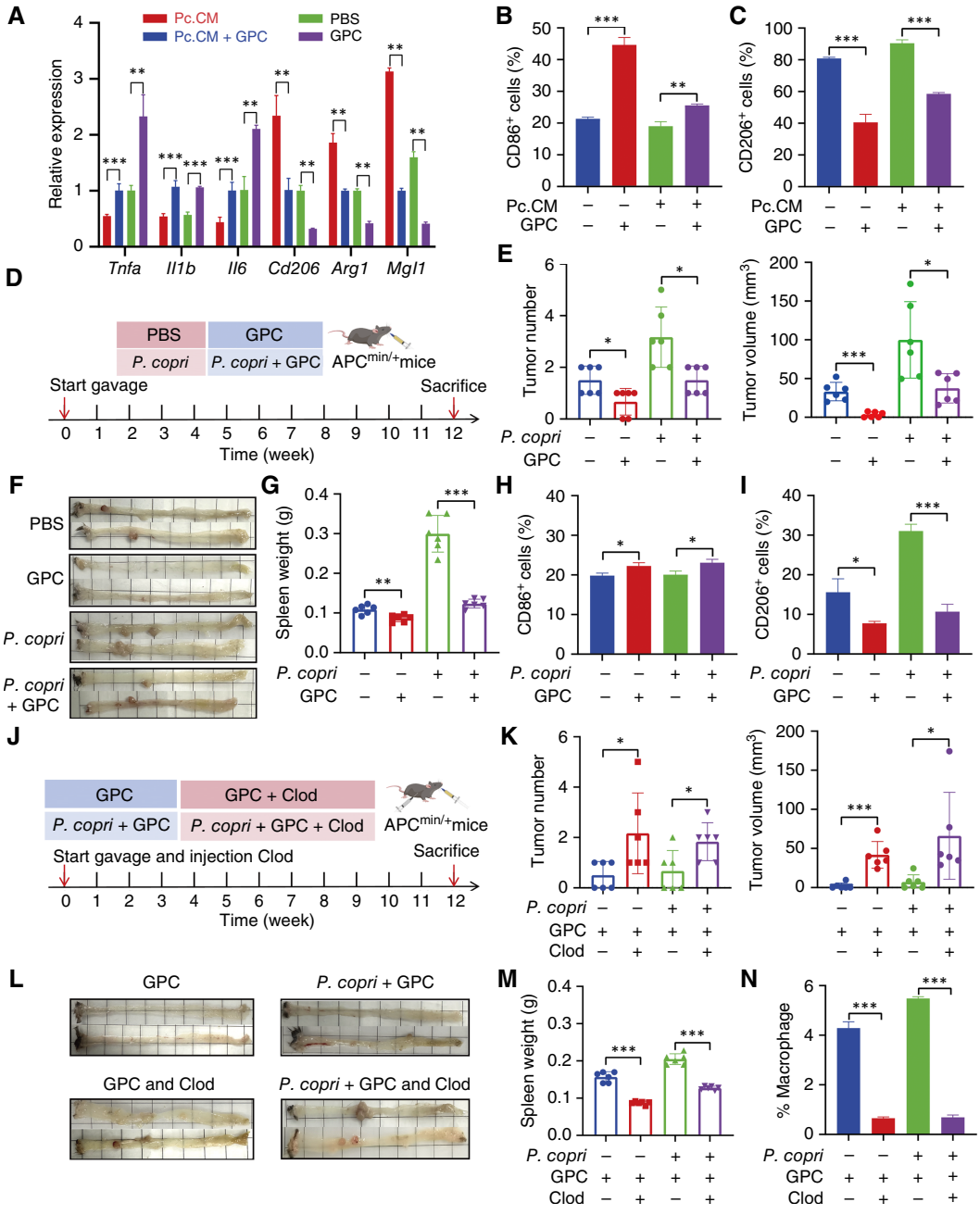

Figure 6.

Supplementation with GPC suppresses colorectal cancer progression induced by *P. copri* by regulating macrophage polarization. **A,** The expression of macrophage-related genes in THP-1–derived macrophages following Pc.CM, GPC, or Pc.CM + GPC stimulation. **B** and **C,** The proportion of CD86$^+$ macrophages (**B**) and CD206$^+$ macrophages (**C**). **D,** APC$^{min/+}$ mice received oral gavage of *P. copri*, GPC, or *P. copri* + GPC for 12 weeks ($n = 6$ per group). **E–G,** Tumor number and volume (**E**), representative images of colon (**F**), and spleen weight (**G**) in APC$^{min/+}$ mice treated with *P. copri*, GPC, or *P. copri* + GPC. **H** and **I,** The proportion of CD86$^+$ macrophages (**H**) and CD206$^+$ macrophages (**I**) in tumors from APC$^{min/+}$ mice treated with *P. copri*, GPC, or *P. copri* + GPC. **J,** APC$^{min/+}$ mice received GPC and *P. copri* with weekly clodronate (Clod) liposome injections for macrophage depletion ($n = 6$ per group). **K–N,** Tumor number and volume (**K**), representative images of colon (**L**), spleen weight (**M**), and percentage of macrophage (**N**) in APC$^{min/+}$ mice. Data are expressed as mean ± SD, *, $P < 0.05$; **, $P < 0.01$; ***, $P < 0.001$.

depletion markedly increased colorectal tumor burden and abrogated the tumor-suppressive effects of GPC treatment (**Fig. 6K–N**). This suggests that GPC is the key substance through which *P. copri* regulates macrophage polarization.

GPC suppresses colorectal cancer progression via MARCO$^+$ macrophages

Given that many lipid molecules exert biological effects via interaction with immune cell surface (19, 20), we employed molecular

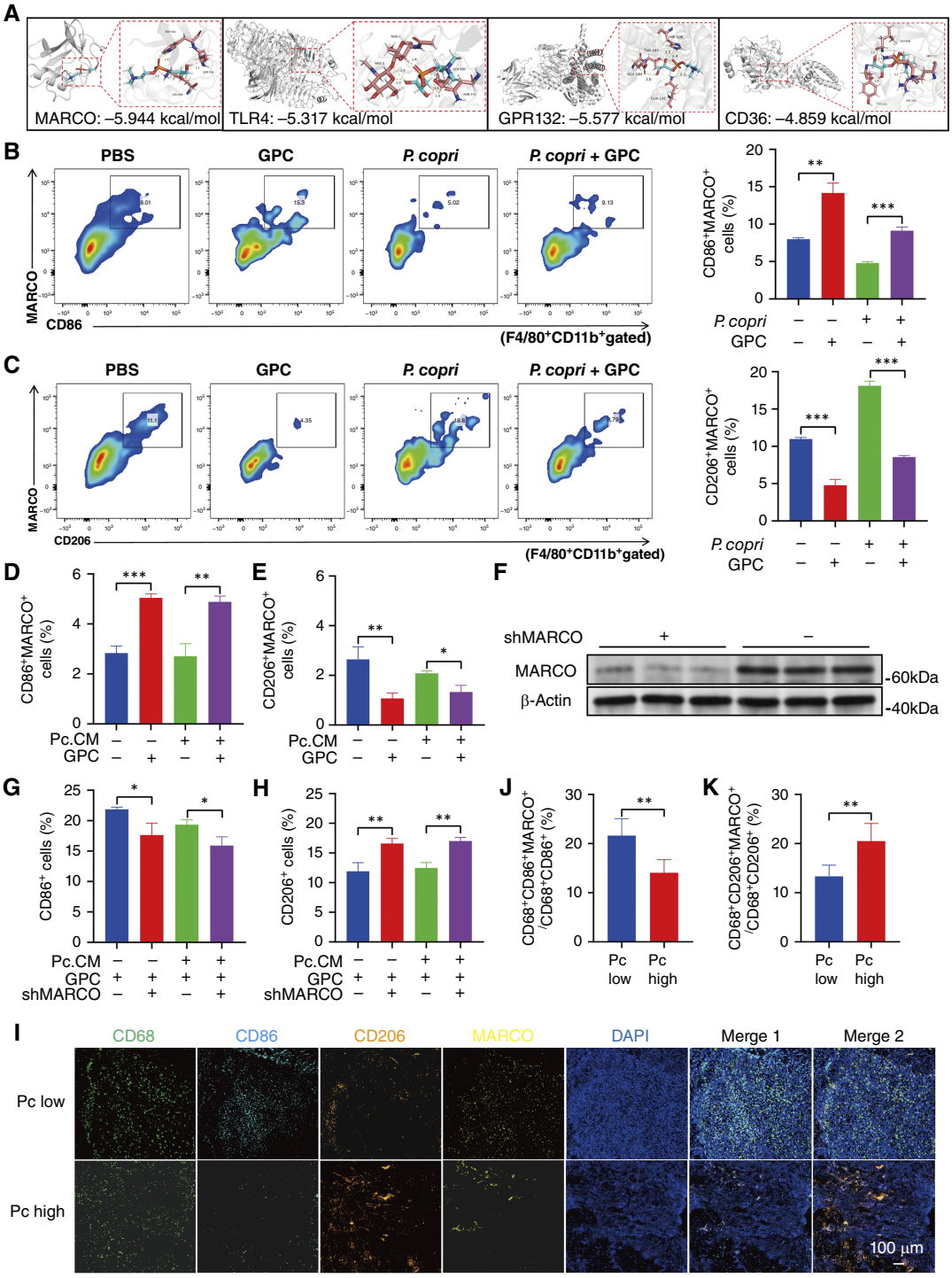

Figure 7.

Potential mechanism of GPC in regulating macrophage polarization. **A,** Molecular docking analysis identifies potential receptor for GPC binding. **B** and **C,** MARCO$^+$ CD86$^+$ macrophages (**B**) and MARCO$^+$ CD206$^+$ macrophages (**C**) in tumors from APC$^{min/+}$ mice treated with *P. copri*, GPC, or *P. copri* + GPC. **D** and **E,** The proportion of MARCO$^+$ CD86$^+$ macrophages (**D**) and MARCO$^+$ CD206$^+$ macrophages (**E**) in BMDMs treated with Pc.CM, GPC, or Pc.CM + GPC. **F,** The expression of MARCO protein in BMDMs infected by MARCO lentivirus. **G** and **H,** The proportion of CD86$^+$ macrophages (**G**) and CD206$^+$ macrophages (**H**) in BMDMs treated with Pc.CM, GPC, or shMacro. **I–K,** Immunofluorescence of TAMs in human colorectal cancer tissues with high vs. low *P. copri* signal intensity. Merge 1, CD68/CD86/MARCO/DAPI; merge 2, CD68/CD206/MARCO/DAPI. Data are expressed as mean ± SD, *, $P < 0.05$; **, $P < 0.01$; ***, $P < 0.001$.

docking to explore whether GPC interacts with macrophage receptors (21). Among the screened candidates, MARCO emerged as the top-ranking target based on docking affinity (**Fig. 7A**). Previous studies suggest that MARCO$^+$ macrophages are associated with immunosuppression and may play a crucial role in tumor progression and treatment response (22, 23). In our animal experiments, GPC administration significantly increased MARCO$^+$ M1-like macrophages and decreased MARCO$^+$ M2-like subsets in APC$^{min/+}$ mice, both in the presence and absence of *P. copri* colonization (**Fig. 7B** and **C**). These findings were further validated in BMDMs treated with GPC *in vitro* (**Fig. 7D** and **E**). Together, these data indicate that GPC inhibits the tumor-promoting phenotype of MARCO$^+$ macrophages and reshapes the immunosuppressive TME, thereby exerting protective effects against *P. copri*–induced colorectal cancer progression. To confirm the role of MARCO in mediating GPC-induced macrophage polarization, we performed MARCO knockdown using lentiviral transfection in BMDMs. Notably, MARCO silencing abrogated the polarization of BMDMs induced by GPC (**Fig. 7F–H**), functionally validating MARCO as a key cellular target of GPC. Importantly, in human colorectal cancer tissues, high *P. copri* abundance coincided with decreased MARCO$^+$ M1-like TAMs and increased MARCO$^+$ M2-like TAMs (**Fig. 7I–K**), further validating the clinical relevance of this axis. These findings uncover MARCO's previously unrecognized role in mediating *P. copri*–induced TAM polarization during colorectal cancer progression.

Discussion

The intestinal environment in which colorectal cancer develops is among the most microbially complex ecosystems in the human body. Recent studies have increasingly emphasized the pivotal role of both tissue-resident and gut microbiota in tumor initiation and progression (24). To date, substantial research has characterized the microbial profiles of tumor-resident and gut microbiota in patients with colorectal cancer. In colorectal cancer tissues, enrichment of *Fusobacterium nucleatum* and depletion of *Leptotrichia* family bacteria have been associated with modulation of cancer progression (25). Moreover, analysis of the tumor microbiota has demonstrated significant prognostic value for predicting colorectal cancer outcomes (26, 27). In this study, we observed significant differences in intratumoral microbial diversity across various tumor stages in patients with colorectal cancer. Notably, we not only found that *Prevotella* is a significant member of the TME but also observed that it was markedly enriched in advanced T-stage tumors. Furthermore, the tumor and adjacent normal tissues actually constitute two distinct environments. By analyzing the microbial populations in these two areas and applying the theory of community assembly (8, 10), we have preliminarily concluded that a microbial community, including *Prevotella*, migrates into the TME with tumor progression, with *P. copri*'s parenchymal invasion conclusively demonstrated by FISH. These findings indicate that intratumoral *Prevotella* may have significant potential in the progression and outcomes of colorectal cancer.

Prevotella, a Gram-negative anaerobic bacterium first identified in 1990 (28), is a common and abundant member of the human microbiota, colonizing multiple body sites, including the gastrointestinal tract, oral cavity, and vagina (29). Among gut-associated *Prevotella* species, *P. copri* is the most prominent. Previous studies have linked *P. copri* to deleterious effects under inflammatory conditions, such as rheumatoid arthritis and ankylosing spondylitis (30). Moreover, *P. copri* has been shown to be enriched in Eastern populations and is closely linked to dietary habits and disease development in this demographic (31, 32). Studies have demonstrated that *P. copri* can activate the TLR4–ZFP90–NFκB signaling pathway and promote colorectal cancer progression in mice (33). However, the role of *P. copri* within tumors and its specific mechanisms of action in the TME remain largely unclear. Here, we demonstrated that *P. copri* promotes tumor growth in multiple murine models, including oral gavage and an intratumoral bacterial model, providing the first comprehensive evidence of *P. copri* contributing to colorectal cancer progression from the TME perspective.

Previous study illustrated that bacteria can exert effects through their structural components or metabolic products, such as lipopolysaccharide from gut microbiota (34) or indole-3-lactic acid produced by bacterial metabolism (35). In addition, microbiota can also participate in the host metabolic process, such as the urea cycle (36), or directly regulate the expression of metabolic enzymes (37). With both *in vivo* and *in vitro* untargeted metabolomics profiling, our study identified GPC as the only overlapping differentially abundant metabolite. GPC, a water-soluble acetylcholine precursor with recognized nutraceutical potential, is approved for use in cognitive health and has been shown to modulate immune responses (38, 39). Although GPC has been primarily studied in the context of neuropsychiatric disorders, such as cognitive impairment (40) and neuronal injury after seizure (41), our findings represent the first demonstration and validation of GPC's role in improving colorectal cancer outcomes, linking intratumoral bacteria with intratumoral metabolism. Given this, we propose that in the context of colorectal cancer, *P. copri* exerts its influence through a dual identity (42): as a gut commensal, it competes with the host for GPC, thereby reducing systemic levels that indirectly affect the tumor, and as an intratumoral resident, it directly depletes GPC within the local microenvironment. This dual role coherently explains the observed systemic GPC reduction and its local impact on tumor.

Emerging evidence has shown that microbiota can regulate the recruitment, activation, and function of various immune cells within the TME through multiple mechanisms, playing a crucial role in colorectal cancer development, progression, and response to therapy (43). In addition to the microbiota and their metabolites, the TME also comprises a diverse array of immune cells, among which macrophages are critical sentinel immune cells that play essential roles in pathogen defense, antigen presentation, phagocytosis, tissue repair, and tumorigenesis (44). TAMs, the most abundant and highly plastic immune cell population in the TME, are primarily classified into two subtypes: tumor-suppressive M1 macrophages and tumor-promoting M2 macrophages (45, 46). TAM polarization is regulated by the TME, epigenetic modification, and microbiota, collectively influencing colorectal cancer progression (47). Certain bacteria can directly modulate immune cells. For example, *Fusobacterium nucleatum* induces M2 polarization of macrophages to promote colorectal cancer cell liver metastasis (48), and *Anaerococcus digesitans* facilitates M2 macrophage polarization to drive intestinal tumorigenesis (49). Our study further explores the intricate interplay between the intratumoral microbiota, metabolites, and immune cells within the TME. We identified a novel axis involving *P. copri*, GPC, and MARCO$^+$ TAMs that contributes to colorectal cancer progression. Specifically, *P. copri* influences the TME by modulating the levels of GPC, a metabolite that affects the polarization of TAMs towards a tumor-suppressive M1 phenotype. This *P. copri*–GPC–MARCO$^+$ TAM axis represents a previously

unrecognized immunomodulatory pathway in colorectal cancer, highlighting the complex interconnections within the TME that drive tumor progression.

Although this study advances understanding of *P. copri* in colorectal cancer, some limitations remain. First, our FISH analysis, particularly for early-stage (Tis–T2) tumors, was constrained by the limited availability of such surgical specimens at our institution. Future studies involving collaboration with endoscopy centers or multicenter cohorts will be essential to validate and extend these spatial observations across the full spectrum of colorectal cancer stages. Second, we could not track real-time bacterial migration routes or determine translocation mechanisms. Moreover, the clinical relevance of GPC depletion and its association with MARCO$^+$ TAMs, as well as the impact of dietary GPC intake, requires validation in future prospective cohorts. Furthermore, to gain deeper functional insights, we have planned two key follow-up studies: the characterization of *P. copri* strains via metagenomic sequencing and enzymological assays and an investigation into the subtle differences of *P. copri* strains across different anatomic niches. These limitations will guide future longitudinal clinical studies and refine experimental models to fully elucidate *P. copri*'s pathogenic mechanisms in colorectal cancer.

In summary, we identify *P. copri* as a tumor-enriched bacterium in patients with colorectal cancer and a potential driver of tumor progression. By analyzing paired tumor and adjacent samples across tumor stages, we uncover a dynamic, stage-dependent microbial migration pattern that favors *P. copri* accumulation within the TMEs. Mechanistically, *P. copri* depletes local GPC pools to reprogram MARCO$^+$ TAMs, promoting an immunosuppressive TME conducive to tumor growth. These findings highlight a potential therapeutic axis involving microbial metabolism, macrophage plasticity, and tumor immunity in colorectal cancer, providing a foundation for the development of novel targeted therapies that modulate the TME.

Data Availability

The 16S rRNA sequencing and RNA sequencing data generated in this study were uploaded to the National Genomics Data Center database, with Bioproject number PRJCA040185. Publicly available metagenomic data analyzed in this study were obtained from the European Nucleotide Archive at PRJEB7774 and PRJDB4176. All other raw data generated in this study are available upon request from the corresponding author.

Authors' Disclosures

No disclosures were reported.

Authors' Contributions

Q. Yuan: Conceptualization, data curation, formal analysis, validation, investigation, visualization, methodology, writing–original draft, project administration, writing–review and editing. **Y. Sun:** Investigation, visualization, methodology. **Y. Zhang:** Investigation, methodology. **C. Chen:** Investigation, methodology. **C. Bu:** Investigation. **X. Hua:** Investigation. **L. Sun:** Resources, supervision, investigation, methodology. **Y. Sun:** Resources, supervision, funding acquisition. **Z. Zhang:** Conceptualization, resources, supervision, funding acquisition, validation, writing–original draft, project administration, writing–review and editing. **Y. Feng:** Conceptualization, resources, data curation, supervision, funding acquisition, validation, project administration, writing–review and editing.

Acknowledgments

We thank the patients who generously donated their samples for this study. All investigations involving human subjects were conducted in accordance with government policies and the Declaration of Helsinki. We acknowledge the Core Facility of The First Affiliated Hospital of Nanjing Medical University for its technical support. This work was funded by National Natural Science Foundation of China (82372641 and 82373627) and Basic Research Program of Jiangsu (no. BK20251855).

Note

Supplementary data for this article are available at Cancer Research Online (http://cancerres.aacrjournals.org/).

Received August 1, 2025; revised November 13, 2025; accepted January 21, 2026; posted first January 27, 2026.

References

1. Siegel RL, Giaquinto AN, Jemal A. Cancer statistics, 2024. CA Cancer J Clin 2024;74:12–49.
2. Eng C, Yoshino T, Ruíz-García E, Mostafa N, Cann CG, O'Brian B, et al. Colorectal cancer. Lancet 2024;404:294–310.
3. Murphy CC, Zaki TA. Changing epidemiology of colorectal cancer - birth cohort effects and emerging risk factors. Nat Rev Gastroenterol Hepatol 2024;21:25–34.
4. Sung H, Siegel RL, Laversanne M, Jiang C, Morgan E, Zahwe M, et al. Colorectal cancer incidence trends in younger versus older adults: an analysis of population-based cancer registry data. Lancet Oncol 2025;26:51–63.
5. Zhou Y, Bian S, Zhou X, Cui Y, Wang W, Wen L, et al. Single-cell multiomics sequencing reveals prevalent genomic alterations in tumor stromal cells of human colorectal cancer. Cancer Cell 2020;38:818–28.e5.
6. Nejman D, Livyatan I, Fuks G, Gavert N, Zwang Y, Geller LT, et al. The human tumor microbiome is composed of tumor type-specific intracellular bacteria. Science 2020;368:973–80.
7. Fu A, Yao B, Dong T, Chen Y, Yao J, Liu Y, et al. Tumor-resident intracellular microbiota promotes metastatic colonization in breast cancer. Cell 2022;185:1356–72.e26.
8. Liao Y, Wu Y-X, Tang M, Chen Y-W, Xie J-R, Du Y, et al. Microbes translocation from oral cavity to nasopharyngeal carcinoma in patients. Nat Commun 2024;15:1645.
9. Sloan WT, Lunn M, Woodcock S, Head IM, Nee S, Curtis TP. Quantifying the roles of immigration and chance in shaping prokaryote community structure. Environ Microbiol 2006;8:732–40.
10. Yang Q, Zhang P, Li X, Yang S, Chao X, Liu H, et al. Distribution patterns and community assembly processes of eukaryotic microorganisms along an altitudinal gradient in the middle reaches of the Yarlung Zangbo River. Water Res 2023;239:120047.
11. Zhang J, Wu Y, Liu J, Yang Y, Li H, Wu X, et al. Differential oral microbial input determines two microbiota pneumo-types associated with health status. Adv Sci (Weinh) 2022;9:e2203115.
12. Xiong X, Chen S, Shen J, You H, Yang H, Yan C, et al. Cannabis suppresses antitumor immunity by inhibiting JAK/STAT signaling in T cells through CNR2. Signal Transduct Target Ther 2022;7:99.
13. Zhang Z, Chen C, Yang F, Zeng YX, Sun P, Liu P, et al. Itaconate is a lysosomal inducer that promotes antibacterial innate immunity. Mol Cell 2022;82:2844–57.e10.
14. Cai J, Peng J, Zang X, Feng J, Li R, Ren P, et al. Mammary leukocyte-assisted nanoparticle transport enhances targeted milk trace mineral delivery. Adv Sci (Weinh) 2022;9:e2200841.
15. Bu L, Gao M, Qu S, Liu D. Intraperitoneal injection of clodronate liposomes eliminates visceral adipose macrophages and blocks high-fat diet-induced weight gain and development of insulin resistance. AAPS J 2013;15:1001–11.
16. Su J, Lin X, Li D, Yang C, Lv S, Chen X, et al. Prevotella copri exhausts intrinsic indole-3-pyruvic acid in the host to promote breast cancer progression: inactivation of AMPK via UHRF1-mediated negative regulation. Gut Microbes 2024;16:2347757.
17. Abdelsalam NA, Hegazy SM, Aziz RK. The curious case of Prevotella copri. Gut Microbes 2023;15:2249152.
18. Hezaveh K, Shinde RS, Klötgen A, Halaby MJ, Lamorte S, Ciudad MT, et al. Tryptophan-derived microbial metabolites activate the aryl hydrocarbon receptor in tumor-associated macrophages to suppress anti-tumor immunity. Immunity 2022;55:324–40 e8.

19. Liu P, Zhu W, Chen C, Yan B, Zhu L, Chen X, et al. The mechanisms of lysophosphatidylcholine in the development of diseases. Life Sci 2020;247:117443.
20. Liang S, Zhou J, Cao C, Liu Y, Ming S, Liu X, et al. GITR exacerbates lysophosphatidylcholine-induced macrophage pyroptosis in sepsis via post-translational regulation of NLRP3. Cell Mol Immunol 2024;21:674–88.
21. Paggi JM, Pandit A, Dror RO. The art and science of molecular docking. Annu Rev Biochem 2024;93:389–410.
22. Ding L, Qian J, Yu X, Wu Q, Mao J, Liu X, et al. Blocking MARCO^{+} tumor-associated macrophages improves anti-PD-L1 therapy of hepatocellular carcinoma by promoting the activation of STING-IFN type I pathway. Cancer Lett 2024;582:216568.
23. La Fleur L, Botling J, He F, Pelicano C, Zhou C, He C, et al. Targeting MARCO and IL37R on immunosuppressive macrophages in lung cancer blocks regulatory T cells and supports cytotoxic lymphocyte function. Cancer Res 2021;81:956–67.
24. Dohlman AB, Arguijo Mendoza D, Ding S, Gao M, Dressman H, Iliev ID, et al. The cancer microbiome atlas: a pan-cancer comparative analysis to distinguish tissue-resident microbiota from contaminants. Cell Host Microbe 2021;29:281–98.e5.
25. Zhang X, Yu D, Wu D, Gao X, Shao F, Zhao M, et al. Tissue-resident Lachnospiraceae family bacteria protect against colorectal carcinogenesis by promoting tumor immune surveillance. Cell Host Microbe 2023;31:418–32.e8.
26. Mouradov D, Greenfield P, Li S, In EJ, Storey C, Sakthianandeswaren A, et al. Oncomicrobial community profiling identifies clinicomolecular and prognostic subtypes of colorectal cancer. Gastroenterology 2023;165:104–20.
27. Flemer B, Lynch DB, Brown JMR, Jeffery IB, Ryan FJ, Claesson MJ, et al. Tumour-associated and non-tumour-associated microbiota in colorectal cancer. Gut 2017;66:633–43.
28. Shah HN, Collins DM. Prevotella, a new genus to include Bacteroides melaninogenicus and related species formerly classified in the genus Bacteroides. Int J Syst Bacteriol 1990;40:205–8.
29. Tett A, Pasolli E, Masetti G, Ercolini D, Segata N. Prevotella diversity, niches and interactions with the human host. Nat Rev Microbiol 2021;19:585–99.
30. Alpizar-Rodriguez D, Lesker TR, Gronow A, Gilbert B, Raemy E, Lamacchia C, et al. Prevotella copri in individuals at risk for rheumatoid arthritis. Ann Rheum Dis 2019;78:590–3.
31. Tett A, Huang KD, Asnicar F, Fehlner-Peach H, Pasolli E, Karcher N, et al. The Prevotella copri complex comprises four distinct clades underrepresented in westernized populations. Cell Host Microbe 2019;26:666–79.e7.
32. Huh JW, Kim MJ, Kim J, Lee HG, Ryoo S-B, Ku J-L, et al. Enterotypical Prevotella and three novel bacterial biomarkers in preoperative stool predict the clinical outcome of colorectal cancer. Microbiome 2022;10:203.
33. Han JX, Tao ZH, Qian Y, Yu CY, Li J, Kang ZR, et al. ZFP90 drives the initiation of colitis-associated colorectal cancer via a microbiota-dependent strategy. Gut Microbes 2021;13:1–20.
34. Yang Y, Li L, Xu C, Wang Y, Wang Z, Chen M, et al. Cross-talk between the gut microbiota and monocyte-like macrophages mediates an inflammatory response to promote colitis-associated tumourigenesis. Gut 2020;70:1495–506.
35. Li Y, Li Q, Yuan R, Wang Y, Guo C, Wang L. Bifidobacterium breve-derived indole-3-lactic acid ameliorates colitis-associated tumorigenesis by directing the differentiation of immature colonic macrophages. Theranostics 2024;14:2719–35.
36. Chen H, Tong T, Lu SY, Ji L, Xuan B, Zhao G, et al. Urea cycle activation triggered by host-microbiota maladaptation driving colorectal tumorigenesis. Cell Metab 2023;35:651–66.e7.
37. Fan L, Liu B, Wang Y, Tang B, Xu T, Fu J, et al. Intestinal Lactobacillus murinus-derived small RNAs target porcine polyamine metabolism. Proc Natl Acad Sci U S A 2024;121:e2413241121.
38. Cikes D, Leutner M, Cronin SJF, Novatchkova M, Pfleger L, Klepochová R, et al. Gpcpd1-GPC metabolic pathway is dysfunctional in aging and its deficiency severely perturbs glucose metabolism. Nat Aging 2024;4:80–94.
39. Lu M-S, Fang Y-J, Pan Z-Z, Zhong X, Zheng M-C, Chen Y-M, et al. Choline and betaine intake and colorectal cancer risk in Chinese population: a case-control study. PLoS One 2015;10:e0118661.
40. Sagaro GG, Traini E, Amenta F. Activity of choline alphoscerate on adult-onset cognitive dysfunctions: a systematic review and meta-analysis. J Alzheimers Dis 2023;92:59–70.
41. Lee M, Choi BY, Suh SW. Unexpected effects of acetylcholine precursors on pilocarpine seizure- induced neuronal death. Curr Neuropharmacol 2018;16:51–8.
42. Liao K, Wen J, Liu Z, Zhang B, Zhang X, Fu Y, et al. The role of intratumoral microbiome in the occurrence, proliferation, metastasis of colorectal cancer and its underlying therapeutic strategies. Ageing Res Rev 2025;111:102820.
43. Goenka A, Khan F, Verma B, Sinha P, Dmello CC, Jogalekar MP, et al. Tumor microenvironment signaling and therapeutics in cancer progression. Cancer Commun (Lond) 2023;43:525–61.
44. Matusiak M, Hickey JW, van Ijzendoorn DGP, Lu G, Kidziński L, Zhu S, et al. Spatially segregated macrophage populations predict distinct outcomes in colon cancer. Cancer Discov 2024;14:1418–39.
45. Li X-M, Yang Y, Jiang F-Q, Hu G, Wan S, Yan W-Y, et al. Histone lactylation inhibits RARγ expression in macrophages to promote colorectal tumorigenesis through activation of TRAF6-IL-6-STAT3 signaling. Cell Rep 2024;43:113688.
46. Yan H, Wang Z, Teng D, Chen X, Zhu Z, Chen H, et al. Hexokinase 2 senses fructose in tumor-associated macrophages to promote colorectal cancer growth. Cell Metab 2024;36:2449–67.e6.
47. El Tekle G, Andreeva N, Garrett WS. The role of the microbiome in the etiopathogenesis of colon cancer. Annu Rev Physiol 2024;86:453–78.
48. Xu C, Fan L, Lin Y, Shen W, Qi Y, Zhang Y, et al. Fusobacterium nucleatum promotes colorectal cancer metastasis through miR-1322/CCL20 axis and M2 polarization. Gut Microbes 2021;13:1980347.
49. Long X, Wong CC, Tong L, Chu ESH, Ho Szeto C, Go MYY, et al. Peptostreptococcus anaerobius promotes colorectal carcinogenesis and modulates tumour immunity. Nat Microbiol 2019;4:2319–30.